

Forecasting neutron star temperatures: predictability and variability

Dany Page¹ and Sanjay Reddy²

¹*Instituto de Astronomía, Universidad Nacional Autónoma de México, Mexico D.F. 04510, Mexico*

²*Institute for Nuclear Theory, University of Washington, Seattle, Washington 98195, USA*

It is now possible to model thermal relaxation of neutron stars after bouts of accretion during which the star is heated out of equilibrium by nuclear reactions in its crust. Major uncertainties in these models can be encapsulated in modest variations of a handful of fudge parameters that change the crustal thermal conductivity, specific heat, and heating rates. Observations of thermal relaxation constrain these fudge parameters and allow us to predict longer term variability in terms of the neutron star core temperature. We demonstrate this explicitly by modeling ongoing thermal relaxation in the neutron star XTE J1701-462. Its future cooling, over the next 5 to 30 years, is strongly constrained and depends mostly on its core temperature, uncertainties in crust physics having essentially been pinned down by fitting to the first three years of observations.

PACS numbers: 26.60.Gj, 97.60.Jd, 97.80.Jp, 98.70.Qy

Neutron star-low mass x-ray binaries (NS-LMXBs) are close binary systems in which a neutron star is accreting matter from a low-mass companion through Roche lobe overflow [1]. In many systems accretion is not continuous, and during quiescence, when presumably no, or very little, accretion is occurring, thermal radiation from the neutron star surface can be observed to infer its temperature, T_e [2]. In recent years, five NS-LMXBs were observed to return to quiescence after a long accretion outburst that lasted years (1.3 to 24) and have been called quasi-persistent transients (QPTs) [3–5]. Recent attempts to model the observed evolution of T_e after the end of an accretion outburst have revealed that its temporal characteristics are likely set by processes in the outer 1 – 2 km region of the neutron star called the crust [6–8].

During accretion, the gravitational energy released at the surface is radiated away but non-equilibrium reactions occurring deep inside the crust heat the neutron star interior. These reactions arise as accretion induced compression of matter drives electron captures, neutron emissions and absorptions, and pycno-nuclear (i.e., induced by pressure) fusion reactions [9, 10]. Together, these processes liberate about 1.5 – 2 MeV of energy per accreted baryon in the density interval $10^9 - 10^{14}$ g cm⁻³ [11, 12]. This process, called deep crustal heating [13], gradually heats the whole neutron star interior that will reach a stationary temperature T_0 determined by the long term average mass accretion rate, $\langle \dot{M} \rangle$, and the core neutrino luminosity [14].

On a shorter time scale, characteristic of QPTs, heating during a bout of accretion is strong enough to drive the crust out of thermal equilibrium with the core [15] and cooling observed immediately after should reveal the thermal relaxation of the neutron star crust. Theoretical modeling of the two systems KS 1731-260 and MXB 1659-29 (“KS” and “MXB” hereafter) has confirmed this expectation and shown QPTs are unique laboratories for studying neutron star crust physics [6, 7]. Although mat-

ter in the crust is at high density ($\rho \simeq 10^9 - 10^{14}$ g cm⁻³) where novel quantum and superfluid behavior is expected, nuclear interactions are fairly well understood at these sub-nuclear densities and a theoretical framework to describe the structure and thermal properties of matter exists [8, 16]. Models of the neutron star crust are now sufficiently advanced that key uncertainties associated with the thermal conductivity, heat capacity and nuclear reactions rates needed to describe thermal relaxation have been identified and studied [17]. More importantly, as we shall discuss later, together theory and observation already constrain the expected range of variation in these quantities.

In this letter, we combine a detailed theory of the crust with previous constraints and early time cooling data from a specific source XTE J1701-462 (“XTE” hereafter) to make predictions for the future evolution of its surface temperature. Our predictions can be tested in the near term and we find that further cooling is very strongly correlated with its core temperature. In the long term, as additional sources entering a transient cooling phase are discovered, they will further test theoretical predictions and establish the basic paradigm that observed cooling is due to thermal and transport phenomena in the crust. Our numerical simulations use the code *NSCool* [18], an updated version of the code used in [14].

Evolution of temperature in the crust is determined by the heat diffusion equation

$$C_V \frac{\partial T}{\partial t} = \kappa \frac{\partial^2 T}{\partial r^2} + \frac{1}{r^2} \frac{\partial(r^2 \kappa)}{\partial r} \frac{\partial T}{\partial r} + Q_h - Q_\nu \quad (1)$$

where C_V is the specific heat, κ the thermal conductivity, and the other factors, denoted by Q_h and Q_ν , are the nuclear heating and the neutrino cooling rates, respectively. These density and temperature dependent inputs have been studied in some detail. These dependencies are now well fairly understood (for a recent review see [8]) and major uncertainties can be parameterized in terms of a handful of density dependent effective param-

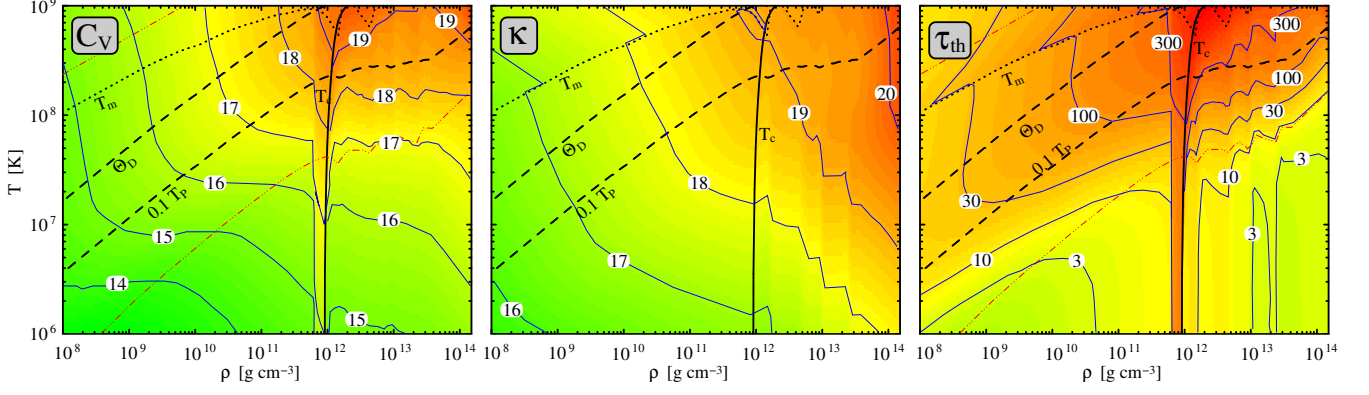


FIG. 1. The “neutron star crust landscape”. Left panel: color plot of the specific heat C_V , in $\text{erg K}^{-1}\text{cm}^{-3}$, with (blue) contour lines labelled by $\log_{10} C_V$. Central panel: color plot of thermal conductivity κ , in $\text{erg K}^{-1}\text{cm}^{-1}\text{s}^{-1}$, with (blue) contour lines labelled by $\log_{10} \kappa$. Right panel: color plot of $\tau_{\text{th}} = C_V/\kappa$ in $\text{time}/(\text{length})^2$ with (blue) contour lines at 3, 10, 30, 100, and 300 days per $(100 \text{ m})^2$. In all three panels $Q_{\text{imp}}^{\text{lo}\rho} = 20$ at ρ below $10^{12} \text{ g cm}^{-3}$ and $Q_{\text{imp}}^{\text{hi}\rho} = 4$ above $10^{13} \text{ g cm}^{-3}$, with a smooth transition inbetween. The neutron $^1\text{S}_0$ gap is from [19] which has a layer of unpaired neutron only just above neutron drip: its T_c is shown. Also plotted on each panel is the ion melting temperature, T_m [20], the Debye temperature $\Theta_D \simeq 0.45 T_P$ [21], and $0.1 T_P$, T_P being the ion plasma temperature. In the C_V and τ_{th} panels, the two (red) dash-triple dot lines demarks the boundaries between which C_V is dominated by the ions.

eters: (i) the local effective ion-plasma frequency $\omega_P = (4\pi Z^2 e^2 n_{\text{ion}}/M_{\text{ion}}^*)^{1/2}$, where n_{ion} is the total ion density and M_{ion}^* is the ion effective mass which incorporates effects due to entrainment in the inner crust [22], Ze being the ion electric charge; (ii) the transition temperature T_c for neutron superfluidity in the inner crust and (iii) the impurity parameter $Q_{\text{imp}} = \sum_i n_i (Z_i - \langle Z \rangle)^2 / n_{\text{ion}}$ where n_i is the number density of the impurity species “ i ” of charge $Z_i e$, $\langle Z \rangle e$ being the average ion charge. Nuclear reactions that generate heat have been also studied and here we employ the heating rates from electron capture and pycno-nuclear reactions from [11, 12]. Despite large uncertainties in the pycno-nuclear reaction rates, the net heating is rather well constrained by global energetics [12].

Due to its high thermal conductivity the core temperature remains nearly uniform and its evolution is slow due to the high specific heat. Consequently, the thermal time-scale is largely set by the crust. A simple estimate gives

$$\tau_{\text{th}} \sim \frac{C_V}{\kappa} (\Delta r)^2 \quad (2)$$

where Δr is the thickness of the evolving layer. An example of the variation of C_V , κ and the ratio C_V/κ are shown in the left, middle and right panels of Fig. 1, respectively. We will now briefly discuss the main sources of uncertainty for C_V and κ and the range of their variability that we will employ in our simulations.

The ions form a quantum Coulomb crystal at low temperature when $T < 0.1 T_P$ where $T_P = \hbar \omega_P / k_B$ is the ion plasma temperature. At these low temperatures, the ion component specific heat is dominated by

the transverse phonons contribution and $C_V^{\text{ion}} \propto T^3/v_t^3$ where $v_t \propto \omega_P/q_D$ is the transverse phonon velocity and $q_D = (6\pi^2 n_{\text{ion}})^{1/3}$ the Debye momentum. The velocity of phonon modes remains somewhat uncertain because coupling between dynamics of the neutron superfluid and the lattice is not known precisely and results in significant variation of C_V^{ion} [22, 23]. We incorporate this uncertainty by considering, at each depth in the inner crust, a range of possible ion effective mass M_{ion}^* , and hence a range of ω_P , from $A m_n$ to $A_{\text{cell}} m_n$, where $A_{\text{cell}} = A + A_{\text{drip}}$, A being the ion mass number and A_{drip} the number of dripped neutron in the Wigner-Seitz cell. When $\Theta_D \lesssim T \lesssim T_m$, T_m being the ion melting temperature, the ion specific heat C_V^{ion} is almost T -independent and $\simeq 3k_B$ while it slowly decreases in the liquid phase. In contrast, the electron component is well approximated by a degenerate ultra-relativistic Fermi-Dirac gas so that the electron specific heat is simply $C_V^e = T p_{\text{Fe}}^2 (k_B^2 / 3 \hbar^2 c)$, where p_{Fe} is the electron Fermi momentum. For $T \ll T_P$ electrons dominate since $C_V^e \propto T$ but with increasing T ions take over, since $C_V^{\text{ion}} \propto T^3$. In the inner crust, neutrons are superfluid below a critical temperature denoted by T_c and their contribution to C_V is suppressed by the factor $\propto \exp(-T/T_c)$ for $T \ll T_c$, and somewhat enhanced near $T \simeq T_c$ [24]. Generically, in a thin layer from the neutron drip point $\rho_{\text{drip}} \simeq 6 \times 10^{11} \text{ g cm}^{-3}$ up to $\sim 10^{12} \text{ g cm}^{-3}$, where $T \gtrsim T_c$, the neutron contribution is large and accounts for the C_V barrier seen in the left and right panels of Fig. 1.

Electrons dominate thermal conduction and their contribution is given by $\kappa_e = C_V^e c^2 / (3 \nu^e)$ where ν^e is the electron scattering rate. When $T \lesssim T_P$ the scattering

rate is dominated by impurity scattering, even for relatively small values of the impurity parameter $Q_{\text{imp}} \sim 1$. The electron-impurity scattering rate is given by

$$\nu_{\text{imp}}^e = \nu_0^e \frac{Q_{\text{imp}}}{\langle Z^2 \rangle} \Lambda_{\text{imp}} \quad (3)$$

where $\nu_0^e = 4\alpha_{\text{em}}^2 \langle Z^2 \rangle p_{\text{Fe}} / (3\pi \langle Z \rangle)$ is the fiducial electron scattering rate in an uncorrelated gas, and $\Lambda_{\text{imp}} \approx 2$ is the Coulomb logarithm for randomly distributed impurities [25]. The elastic impurity scattering rate is independent of temperature and relatively insensitive to lattice and superfluid dynamics.

At shallow depth Q_{imp} is set by the nuclear reactions at the surface where explosive burning through the r-p process can produce highly impure mix with $Q_{\text{imp}} \simeq 30-100$ [26]. However, several processes including chemical separation due to preferential freezing of large Z elements at the bottom of the ocean, and neutron-rearrangement and pycnonuclear reactions deeper in the inner crust are expected to greatly reduce Q_{imp} in the solid regions of the crust [11, 27, 28]. We treat $Q_{\text{imp}}(\rho)$ as a free parameter and allow a density dependence, with a value $Q_{\text{imp}}^{\text{hi}\rho}$, expected to be small, at high densities and $Q_{\text{imp}}^{\text{lo}\rho}$, that could be much higher, at low densities. Modeling crust relaxation in KS and MXB has shown that $Q_{\text{imp}}^{\text{hi}\rho} \simeq 1-5$ is necessary [7].

Among the five known QPTs, XTE is a peculiar system in that during its 1.6 year long outburst it accreted at a high rate close to the Eddington limit, $\dot{M}_{\text{Edd}} \simeq 2 \times 10^{-8} M_{\odot} \text{ yr}^{-1}$ [29]. For comparison, MXB and KS had accretion outburst that lasted 2.5 and 12.5 years with average \dot{M} of $\sim 0.05\dot{M}_{\text{Edd}}$ and $\sim 0.2\dot{M}_{\text{Edd}}$, respectively [4, 29]. The observed cooling light-curves of these three stars are displayed in Fig. 2. XTE's evolution is characterized by a short initial cooling phase of a few hundred days followed by a two year long plateau. This is in sharp contrast to the observed cooling behaviors of KS and MXB that initially evolved on longer time scales of about ~ 300 and ~ 450 days followed by a very slow evolution [3, 31]. Moreover, XTE has, on average, a twice larger T_e^{∞} than MXB and KS, implying that its crust temperature is about four times higher. XTE's evolution explores a new, hotter, regime of the neutron star crust landscape of Fig. 1 which, together with its high $\langle \dot{M} \rangle$ and short outburst, explains its peculiar behavior as we describe below.

We show in Fig. 3, left panel, a series of model crust temperature profiles during accretion induced heating for XTE. The crucial point is that heating was so strong that it would have taken several decades of accretion for XTE to reach a stationary state. A stationary state is reached when the inverted T gradient in the crust is large enough that heat flow into the core exactly balances deep crustal heating. KS and MXB, with lower $\langle \dot{M} \rangle$, could reach a stationary state during their longer outbursts [7].

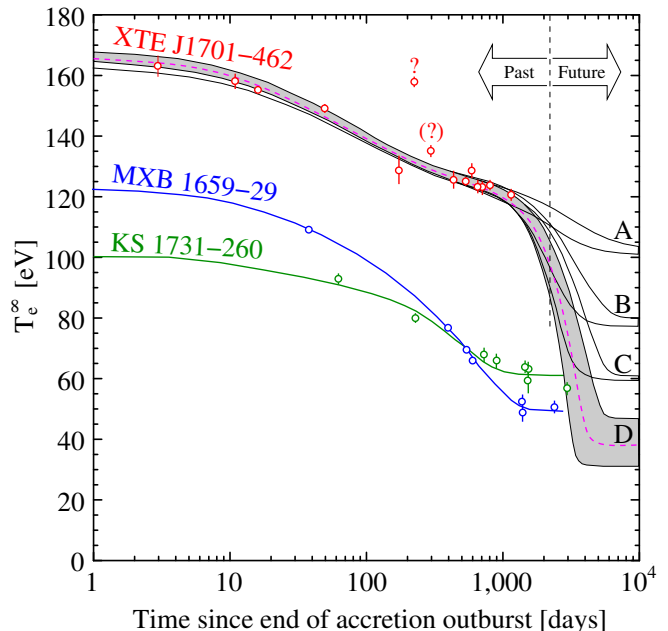


FIG. 2. Observed effective temperatures at infinity, T_e^{∞} (circles with 1σ error bars), after the end of the accretion outburst of KS 1731-260 [3], MXB 1659-29 [4], and XTE J1701-462 [29]. Our theoretical models for KS and MXB, similar to those of [7], employ the crust physics displayed in Fig. 1 but with $(Q_{\text{imp}}^{\text{lo}\rho}, Q_{\text{imp}}^{\text{hi}\rho})$ equal to (5,3) for KS and (10,3) for MXB [30]. The dashed (magenta) curve model for XTE uses exactly the physics of Fig. 1 [30] and details are displayed in Fig. 3. The two data point marked as “?” and “(?)” are likely and possibly, respectively, contaminated by residual accretion [29]. All our models that fit the 12 data points of XTE, up to the last one at 1158 days but excluding the two marked with “?”, are shown in four bands according to the initial core temperature: A: $T_0 = 10^8$ K; B: $T_0 = 10^{7.75}$ K; C: $T_0 = 10^{7.5}$ K, and D that comprises all our models with T_0 between $10^{7.25}$ and 10^6 K. The “Past” and “Future” refer to XTE’s present time.

Crust microphysics displayed in Fig. 1 provides a natural explanation for this diversity - the hotter crust in XTE (where $T \gtrsim 10^8$ K) has larger thermal timescales than those encountered in KS and MXB where $T < 10^8$ K.

The thermal relaxation of XTE after its outburst is illustrated in the right panel of Fig. 3. One sees that the outermost, initially hot, 200 meter thick layer relaxes rapidly, in about 100 days, which results in the observed initial rapid decrease of T_e^{∞} . This time scale roughly matches the thermal time scale $\tau_{\text{th}} \sim 30-100$ days of this layer at $T \sim 2 \times 10^8$ K seen in the right panel of Fig. 1. Subsequent temperature evolution is slow: heat from the outer crust, whose temperature determines the observed T_e^{∞} , has to flow into the inner crust, and then into the core. It has to pass through the bottleneck just above neutron drip where τ_{th} is ~ 1 year at $T \simeq 10^8$ K, and then diffuse several hundreds of meters down to the core. This process explains the existence of a plateau in

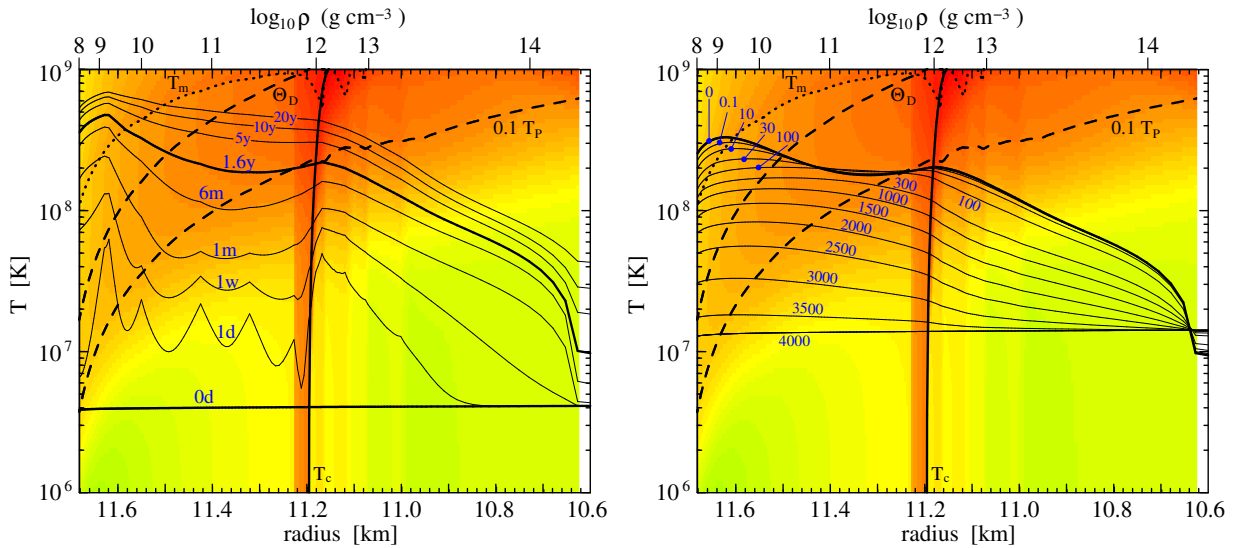


FIG. 3. Left panel: an example of evolution of XTE’s crust temperature during an accretion phase at $\dot{M} \simeq 0.9\dot{M}_{\text{Edd}}$ with initial uniform $T = 4 \times 10^6$ K (labelled “0d”). Profiles after 1 day (“1d”), 1 week (“1w”), 1 and 6 months (“1m” and “6m”) and 1.6 year (“1.6y”) are shown. The profiles at 5, 10 and 20 years (“5y”, “10y” and “20y”) show the times needed to approach the steady state. Right panel: An example of the evolution of XTE’s crust temperature profile during the cooling phase. In both panels the background color map is the local thermal time from Fig. 1. Notice that the core temperature is increasing both during the accretion phase and the subsequent relaxation phase.

the observed T_e^∞ . However, on a longer time scale beyond presently published observations, further decrease of T_e^∞ is naturally expected.

To explore how much three years of observations constrain the properties of the neutron star crust and the future evolution of XTE we performed an extensive search of the parameter space. A comprehensive analysis of our results will be presented in a forthcoming paper but a synopsis is displayed in Fig. 2 as four bands of cooling trajectories labelled as “A” to “D”. The dominant unconstrained parameter is the core temperature and Fig. 2 separates all our models that give a fit to the data with a χ^2 better than 12 in four classes according to their value of T_0 . In the case T_0 is smaller than 10^8 K, fitting the model parameters to the 3 years of observed evolution provides strong constraints and all models in the cases B, C, and D, have crust microphysics very similar to the one depicted in Fig. 1. (The same microphysics is also compatible with modeling of KS and MXB as shown in Fig. 2.) The future evolution of XTE appears to be mostly determined by its previous core temperature T_0 and, for a given T_0 , uncertainty in future time is smaller than a factor of two.

It is remarkable that the crust relaxation model is able to describe vastly different temporal behavior observed in the three sources XTE J1701-462, MXB 1659-29 and KS 1731-260 with very similar input physics in the inner crust. It provides a natural explanation for the rapid early cooling observed in XTE and predicts future cooling solely in terms of one unknown parameter - the core tem-

perature. A robust prediction of the crust cooling model is the correlation between the final temperature and the future cooling rate. Continued monitoring of XTE will be able to test our prediction. If confirmed it would firmly establish the crust relaxation as the underlying process, and taken together fits to these three sources will provide useful constraints for the thermal and transport properties of the neutron star crust. Finally, results displayed in Fig. 3 show that even the core response is not negligible, and these systems may open a new window for studying matter at even larger densities. We hope that the results presented here will motivate a long term program to discover and monitor accreting neutron stars with existing and next generation instruments.

We thank Bob Rutledge for useful discussions at an early stage of this work and Andrew Steiner and Joel Fridriksson for comments on this manuscript. D.P.’s work is partially supported by grants from the UNAM-DGAPA (# IN113211) and Conacyt (CB-2009-01, #132400). D.P. acknowledges the hospitality of the Theoretical Division at the Los Alamos National Laboratory, where part of this work was developed. The work of S.R. was supported by the DOE Grant No. DE-FG02-00ER41132 and by the Topical Collaboration to study *Neutrinos and nucleosynthesis in hot and dense matter*.

-
- [1] M. Van der Klis, in “Compact stellar x-ray sources,” (Cambridge University Press, Cambridge, 2006) p. 39.
- [2] R. E. Rutledge, L. Bildsten, E. F. Brown, G. G. Pavlov, and V. E. Zavlin, *Astrophys. J.*, **514**, 945 (1999).
- [3] E. M. Cackett, E. F. Brown, A. Cumming, N. Degenaar, J. M. Miller, and R. Wijnands, *Astrophys. J. Lett.*, **722**, L137 (2010).
- [4] E. M. Cackett, R. Wijnands, J. M. Miller, E. F. Brown, and N. Degenaar, *Astrophys. J. Lett.*, **687**, L87 (2008).
- [5] J. K. Fridriksson, J. Homan, R. Wijnands, M. Méndez, D. Altamirano, E. M. Cackett, E. F. Brown, T. M. Belloni, N. Degenaar, and W. H. G. Lewin, *Astrophys. J.*, **714**, 270 (2010).
- [6] P. S. Shternin, D. G. Yakovlev, P. Haensel, and A. Y. Potekhin, *Mon. Not. R. Astron. Soc.*, **382**, L43 (2007).
- [7] E. F. Brown and A. Cumming, *Astrophys. J.*, **698**, 1020 (2009).
- [8] D. Page and S. Reddy, in *Neutron Star Crust*, edited by C. A. Bertulani and J. Piekarewicz (Nova Publisher, 2012) arXiv:1201.5602 [nucl-th].
- [9] G. S. Bisnovatyi-Kogan and V. M. Chechetkin, *Soviet Physics Uspekhi*, **127**, 263 (1979).
- [10] P. Haensel and J. L. Zdunik, *Astron. Astrophys.*, **227**, 431 (1990).
- [11] S. S. Gupta, T. Kawano, and P. Moller, *Phys. Rev. Lett.*, **101**, 231101 (2008).
- [12] P. Haensel and J. L. Zdunik, *Astron. Astrophys.*, **480**, 459 (2008).
- [13] E. F. Brown, L. Bildsten, and R. E. Rutledge, *Astrophys. J. Lett.*, **504**, L95 (1998).
- [14] M. Colpi, U. Geppert, D. Page, and A. Possenti, *Astrophys. J. Lett.*, **548**, L175 (2001).
- [15] R. E. Rutledge, L. Bildsten, E. F. Brown, G. G. Pavlov, V. E. Zavlin, and G. Ushomirsky, *Astrophys. J.*, **580**, 413 (2002).
- [16] C. Pethick and D. Ravenhall, *Ann. Rev. Nucl. Part. Sci.*, **45**, 429 (1995).
- [17] N. Chamel and P. Haensel, *Living Reviews in Relativity*, **11**, 10 (2008), arXiv:0812.3955.
- [18] A public version of *NSCool* is available at <http://www.astroscu.unam.mx/neutrones/NSCool/>.
- [19] A. Schwenk, B. Friman, and G. E. Brown, *Nucl. Phys. A*, **713**, 191 (2003).
- [20] W. L. Slattery, G. D. Doolen, and H. E. DeWitt, *Phys. Rev. A*, **26**, 2255 (1982).
- [21] W. J. Carr, *Phys. Rev.*, **122**, 1437 (1961).
- [22] N. Chamel, D. Page, and S. Reddy, *Phys. Rev. C*, **87**, 035803 (2013).
- [23] D. Kobyakov and C. J. Pethick, *Phys. Rev. C*, **87**, 055803 (2013).
- [24] K. P. Levenfish and D. G. Yakovlev, *Astronomy Reports*, **38**, 247 (1994).
- [25] E. Flowers and N. Itoh, *Astrophys. J.*, **206**, 218 (1976).
- [26] H. Schatz, A. Aprahamian, V. Barnard, L. Bildsten, A. Cumming, *et al.*, *Nucl. Phys.*, **A688**, 150 (2001).
- [27] C. J. Horowitz, D. K. Berry, and E. F. Brown, *Phys. Rev. E*, **75**, 066101 (2007).
- [28] A. W. Steiner, *Phys. Rev. C*, **85**, 055804 (2012).
- [29] J. K. Fridriksson, J. Homan, R. Wijnands, E. M. Cackett, D. Altamirano, N. Degenaar, E. F. Brown, M. Méndez, and T. M. Belloni, *Astrophys. J.*, **736**, 162 (2011).
- [30] In agreement with [7] in order to fit the early data points, we need to add an extra energy source at $\rho \sim 10^9 \text{ g cm}^{-3}$. 200 and 100 keV/(accreted nucleon) are enough for KS and XTE. For MXB, however, we need to inject an extra 2MeV/(accreted nucleon) and may indicate that the first observation was contaminated by residual accretion.
- [31] E. M. Cackett, E. F. Brown, A. Cumming, N. Degenaar, J. K. Fridriksson, J. Homan, J. M. Miller, and R. Wijnands, arXiv:1306.1776 [astro-ph.HE].